

Controlling High Harmonic supercontinuum Generation with the spectral polarization of the driver

ELDAR RAGONIS^{1,2}, ERAN BEN-AROSH^{1,2}, LEV MERENSKY^{1,2} AND AVNER FLEISCHER^{1,2,*}

¹Raymond and Beverly Sackler Faculty of Exact Sciences, School of Chemistry, Tel Aviv University, Tel Aviv 6997801, Israel

²Tel-Aviv University center for Light-Matter-Interaction, Tel Aviv 6997801, Israel

*Corresponding author: avnerfleisch@tauex.tau.ac.il

Received XX Month XXXX; revised XX Month, XXXX; accepted XX Month XXXX; posted XX Month XXXX (Doc. ID XXXXX); published XX Month XXXX

We demonstrate a High-Harmonic-Generation (HHG) scheme which offers control of the bandwidth of the spectral peaks. The scheme uses a vectorial two-color driver with close frequencies, generated by spectrally splitting a linearly-polarized input femtosecond-duration laser pulse and subsequent recombining the two halves after their polarizations are made cross-elliptical and counter-rotating. This results in the generation of new emission channels which coalesce into broad HHG peaks, the bandwidth of which increases with photon energy. Liberated from complexities associated with the generation of short driver pulses, this source will find use in HHG applications benefiting from high-flux broadband extreme ultra-violet (XUV) radiation, such as attosecond transient absorption spectroscopy.

High Harmonic Generation (HHG) offers a key tabletop source of extreme ultra violet (XUV) radiation for studies ranging from attosecond science and time-resolved exploration of ultrafast electron dynamics in matter [1-3] to imaging of nanostructures [4-6]. Driving the process by a quasi-monochromatic driver results in the emission of a sparse comb of odd-integer multiples of the driver frequency. Many applications however, e.g. attosecond transient absorption spectroscopy (ATAS) [7-9], require XUV radiation at wavelengths which do not necessarily appear in the comb. This difficulty could be overcome by reducing the number of induced electron recollisions, either by shortening the driver's duration [10], polarization-gating [11-16] or time-gating using a two-color scheme [17-18]. This not only broadens the width of each peak in the comb but possibly also generates a broad supercontinuum at the cutoff energy of the spectrum.

Shortening the driver pulse duration to few- (possibly single-) cycle driver pulses is most commonly done by post-compression techniques where an intense femtosecond-pulse is first spectrally-broadened by the Kerr effect taking place in gas, liquid or solid media followed by subsequent pulse-compression in multilayer chirped mirrors (see [19] and references therein). Different focusing geometries could be used, from unguided free-space focusing through thin solid plates or liquid films, to guided mode in a multi-pass cell or a gas-filled hollow-core capillary (HCF), with the last method still being the most common. With the HCF method [20] the laser peak power, peak intensity and average power must all be kept small enough to ensure that self-focusing, capillary damage or ionization (causing plasma absorption and energy flow to higher-modes) or thermal instabilities (resulting from the absorption of the radiation leaking through the capillary walls) don't occur, respectively. Hence, the HCF method is inherently limited to femtosecond input beams with average power of less than few Watts (see [21] and references therein). When very high or very low average-power laser sources are used, polarization-gating or time-

gating are needed for increasing the bandwidth of the peaks in the HHG spectra (HGS).

Here we add the polarization (spin angular momentum, [22]) degree of freedom to the time-gating technique to obtain a mixed time-polarization-gating technique, which offers continuous controllability over the bandwidth of the harmonic peaks. In our scheme HHG is driven by a vectorial two-color driver with close central frequencies [23], generated by spectrally splitting a linearly-polarized input femtosecond-duration pulse from a commercial amplified Ti:Sa laser and subsequent recombining the two halves after their polarizations are made cross-elliptical and counter-rotating. This considerably broadens the odd peaks in the HGS, which with increasing XUV photon energy could coalesce, yielding a practically continuous HGS. The results are easily explained using a frequency-domain description using photonic channels, which is the picture adopted here. The equivalent, but less intuitive, time-domain description (utilizing the two-dimensional electron trajectories generated by the vectorial field) is described in [24].

A Gaussian pulse whose spectrum $S(\omega) = \exp[-a(\omega - \omega_0)^2]$ is narrow (i.e., $a\omega_0^2 \gg 1$) has the following central frequency $\langle \omega \rangle = \int_0^\infty d\omega \omega S(\omega) / \int_0^\infty d\omega S(\omega) = \omega_0$. When this

input pulse is used to drive HHG, the generated harmonics are odd-integer multiples of the driver's central frequency $\Omega = (2n - 1)\omega_0$ (n is an integer). The spectral width of each harmonic is inversely-proportional to the number of electron recollisions occurring in the process, which is determined by the driver's spectral width. Suppose now this pulse enters a Mach-Zehnder interferometer where the common spectrally-flat beamsplitters are replaced by hard-edge dichroic mirrors which spectrally split (and later recombine) the pulse at ω_0 . Then two pulses exit the interferometer, the central frequency of each being

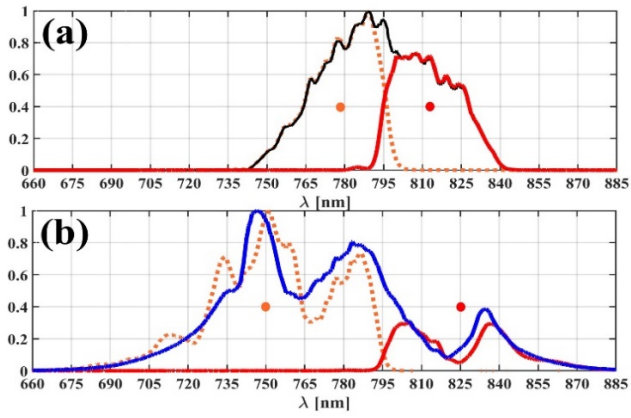


Fig. 1. (a) spectrum of the Ti:Sa laser input pulses entering the interferometer (black) and exiting the interferometer (arm 1- dashed orange, arm 2- solid red). (b) spectrum of the broadened Ti:Sa laser pulses after the HCF (blue) and exiting the interferometer (arm 1- dashed orange, arm 2- solid red). The dichroic mirrors cutoff wavelength is at 795nm. The orange and red dots indicate the central wavelength λ_1 , λ_2 of the pulses from arms 1 and 2, respectively.

$$\omega_1 \equiv \int_{\omega_0}^{\infty} d\omega \omega S(\omega) / \int_{\omega_0}^{\infty} d\omega S(\omega) = \omega_0 + \sqrt{\frac{1}{\pi a}} \quad \text{and}$$

$$\omega_2 \equiv \int_0^{\omega_0} d\omega \omega S(\omega) / \int_0^{\omega_0} d\omega S(\omega) = \omega_0 - \sqrt{\frac{1}{\pi a}}. \text{When a non-}$$

zero time delay is chosen and the two pulses are overlapped in time, a two-color field is obtained. When this field is used to drive HHG, the following harmonic emission channels are obtained [17,22]:

$$\begin{aligned} \Omega_{(n_1, n_2)} &= n_1 \omega_1 + n_2 \omega_2, \quad n_1 + n_2 = 2n - 1 \\ &= (n_1 + n_2) \omega_0 + (n_1 - n_2) \sqrt{\frac{1}{\pi a}} \end{aligned} \quad (1)$$

where n_1, n_2 are integers which refer to the number of annihilated photons from each color ω_1, ω_2 composing the driver. Hence, this simple procedure of spectrally splitting-and-recombining (after slight temporal mismatch) a monochromatic input pulse, generates additional HHG peaks $(n_1 - n_2) \sqrt{\frac{1}{\pi a}}$, the spacing between each

two is controllable by the value of a . For instance, when a is large (small bandwidth of the input pulse), the two frequencies ω_1, ω_2 are close, and the spacing is small. In general, the $(2n-1)^{\text{th}}$ harmonic (in terms of the input pulse central frequency ω_0) that would have been obtained were the HHG process driven by the input pulse, splits into the following set of $2n$ channels $\Omega_{(0, 2n-1)}, \dots, \Omega_{(n, n-1)}, \Omega_{(n+1, n-2)}, \Omega_{(n+2, n-3)}, \dots, \Omega_{(2n-1, 0)}$ when driven by the bichromatic driver. This set covers the energies

$$(2n-1)\omega_0 - (2n-1)\sqrt{\frac{1}{\pi a}} \text{ to } (2n-1)\omega_0 + (2n-1)\sqrt{\frac{1}{\pi a}},$$

yielding a bandwidth of $2(2n-1)\sqrt{\frac{1}{\pi a}}$, which increases with harmonic order (large n).

To demonstrate this experimentally, a commercial amplified Ti:Sa laser (Legend-Elite Duo HE+ USX-5kHz by Coherent) which

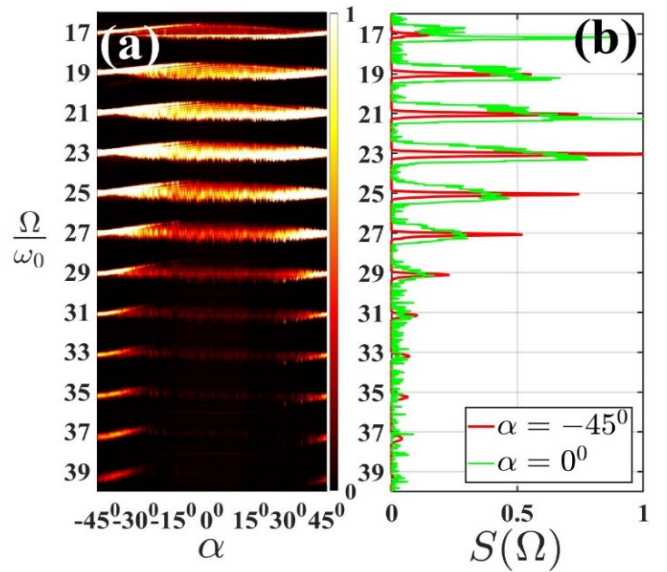


Fig. 2. (a) HGS intensity $S(\Omega)$ (linear scale, normalized to 60000counts/sec) vs. harmonic order and angle α of the achromatic quarter waveplate; The spectrum of the two-color driver which exit the interferometer is given by the orange and red curves of Fig. 1(a). The broad Cooper minima in Argon, around the 33rd harmonic is also visible. (b) HGS lineouts from (a) at $\alpha = -45^\circ$ (red curve) and $\alpha = 0^\circ$ (green curve).

delivers linearly-polarized (horizontal polarization) 25fs, 3mJ pulses at repetition rate of 5kHz is used as input. The laser pulses are spectrally split and recombined in a Mach-Zehnder interferometer whose spectrally-flat beamsplitters were replaced with hard-edge short-pass dichroic mirrors. The dichroic mirrors have a cutoff wavelength at 795nm, around the central wavelength of the Ti:Sa pulses (796.1nm). The interferometer generates two pulses out of each incoming Ti:Sa pulse, with central wavelengths of $\lambda_1 = 777.8\text{nm}$ and $\lambda_2 = 815.2\text{nm}$, respectively which provide an average detuning of $\sqrt{\frac{1}{\pi a}} \approx 0.0235\omega_0$. The spectra of the input

field and the two exit fields are shown in Fig.1a. At the exit of the interferometer the beams are spatially and temporally overlapped (one arm of the interferometer is placed on a motorized linear stage), forming the two-color driver. However, in order to add controllability to this bichromatic HHG scheme, the polarization degree of freedom [22] is utilized, by adding two elements. First, a super-achromatic half waveplate (*B. Halle*) is placed in arm 1 of the interferometer, and flips the linear polarization from horizontal to vertical. Second, at the exit of the interferometer, before entering the HHG generation chamber, the combined beam passes through a super-achromatic quarter-waveplate (*B. Halle*) placed on a motorized rotation stage. As we will show, the orientation α of this waveplate controls the HGS obtained, as the possible emission channels are dictated by spin angular momenta conservation law. In our setup $\alpha = 0^\circ$ corresponds to cross-orthogonal linear-polarizations of the two colors, and $\alpha = \pm 45^\circ$ corresponds to a bicircular counter-rotating driver (the two colors are circularly-polarized with opposite helicities). An intermediate value, i.e., $\alpha = -30^\circ$ corresponds to bielliptical counter rotating driver, with orthogonal major axes of the polarization ellipses.

Using Second Harmonic-Generation Frequency-Resolved Optical

Gating (SHG-FROG) the pulse durations from each arm just prior to the HHG chamber entrance window were measured to be 45fs and 55fs respectively. The energy per pulse in each arm was 440μJ and 480μJ respectively. The two-color driver is focused (using a f=750mm focusing mirror, yielding estimated intensities of $3 \cdot 10^{14} [W/cm^2]$ and $2.7 \cdot 10^{14} [W/cm^2]$ at the jet) few millimeters before a 100μm Argon jet in order to favor the HHG emission from the short trajectories. The resulting XUV radiation is filtered from the remaining infra-red driver radiation with a 0.2μm-thick Aluminum foil. It then enters a home-built HHG spectrometer composed of 50μm by 6mm vertical entrance slit (located 1365mm after the focus), aberration-corrected flat-field concave grating with 300 lines/mm (30-006 by *Shimadzu*), and a back-illuminated CCD camera (Newton DO940P-BN by *Andor*). The spectrometer has a typical resolution of 25meV at 30eV and 90meV at 70eV.

Fig. 2a shows the obtained HGS as function of harmonic order (in units of the frequency ω_0) and the quarter-waveplate reading α .

For $\alpha = -45^\circ$ the driver is bicircular and counter-rotating. Spin angular momenta conservation considerations dictate that only two harmonic channels are possible in this setting: $\Omega_{(n-1,n)}, \Omega_{(n,n-1)}$. These channels are circularly-polarized with opposite helicities. As the reading α increases, each color becomes elliptically-polarized, and supplies the system with circularly-polarized photons of the two possible opposite helicities. In the basis of circular polarization, each channel is characterized by four integers $(n_1^+, n_1^-, n_2^+, n_2^-)$ which refer to the number of annihilated photons from each arm (subscript) and each helicity (superscript). The energy and spin state of harmonic channel $(n_1^+, n_1^-, n_2^+, n_2^-)$ are respectively $\Omega_{(n_1^+, n_1^-, n_2^+, n_2^-)} = (n_1^+ + n_1^-)\omega_1 + (n_2^+ + n_2^-)\omega_2$ and $\sigma_{(n_1^+, n_1^-, n_2^+, n_2^-)} = (n_1^+ + n_2^+) - (n_1^- + n_2^-)$. Hence, the two channels obtained for $\alpha = -45^\circ$ are $\Omega_{(n-1,0,0,n)}, \Omega_{(n,0,0,n-1)}$ and for $\alpha = 45^\circ$ are $\Omega_{(0,n-1,n,0)}, \Omega_{(0,n,n-1,0)}$. As α progresses from $\alpha = -45^\circ$ towards $\alpha = 0^\circ$, higher- and lower- energy channels appear, as also indicated in the diagram in Fig.3c. Note that in this diagram the vertical axis represents the energy of the photonic channel (in units of the detuning $\sqrt{1/\pi\alpha}$) and the horizontal axis is in proportion to the reading α and indicates the number of new circular driver photons n_1^-, n_2^+ . At $\alpha = 0^\circ$ the maximal number of channels is allowed, extending all the way from $\Omega_{(0,0,n-1,n)}, \Omega_{(0,0,n,n-1)}$ to $\Omega_{(n,n-1,0,0)}, \Omega_{(n-1,n,0,0)}$ and the emission support is the largest. This is evident also from Fig.2b in which lineouts from Fig. 2a are shown. With average detuning of $\sqrt{1/\pi\alpha} \approx 0.0235\omega_0$ the anticipated bandwidth covered by the set of $2n$ channels (at $\alpha = 0^\circ$) is $(2n-1)0.047\omega_0$, about $(2n-1)$ -times larger (same as) the measured bandwidth of each odd-integer peak when HHG is driven directly by 25fs (7fs) linearly-polarized input pulses. The measured maximal bandwidth of the 23rd harmonic, is however only 5-times larger than the peak bandwidth

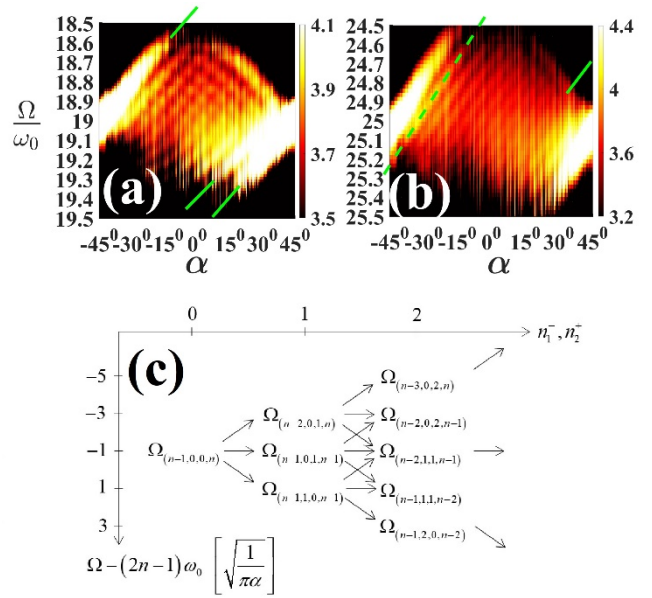


Fig. 3. zoom-in view on the 19th (a) and 25th (b) harmonics of Fig. 2a., showing 10 upward-tilted (and few downward-tilted) bright lines for the 19th harmonic and 13 bright lines for the 25th harmonic. Few of them are marked by solid and dashed green indication lines (c) Diagram representing the birth of harmonic channels as the quarter waveplate reading increases from $\alpha = -45^\circ$. The horizontal axis counts the number of new type of photons n_1^-, n_2^+ supplied to the HHG process when the quarter waveplate is rotated. These photons give rise to new harmonic channels.

at $\alpha = -45^\circ$ (which contains 2 channels), instead of the anticipated ratio of 12. This indicates that not all channels appear in the measurement. While the emission is still peaked around odd-integer multiples of ω_0 , the peak bandwidth is controlled by α , with the effect increasing with harmonic order. Repeating the scans for different delays of the moving arm of the interferometer didn't change these results significantly.

A zoom-in view into the 19th and the 25th harmonics of Fig. 2 is shown in Fig.3 a,b. For the 19th harmonic, the predicted discrete channels are clearly visible. As α is varied, each group of channels emerging from an odd-integer harmonic $19 (2n-1)$ forms a structure of $10 (n)$ upward-tilted bright lines (some of are indicated by green lines) and $9 (n-1)$ dark lines between the bright ones, yielding a total of $19 (2n-1)$ lines. These lines are crossing with $19 (2n-1)$ downward-tilted bright and dark lines, forming a chessboard pattern of bright and dark cells which mark the discrete harmonic channels. Due to limited spectral resolution only 13 upward-tilted bright lines are seen for the 25th harmonic, and no downward-tilted lines. The energy separation of every two cells (bright and black), along the energy axis (for e.g., $\alpha = 0^\circ$) is $0.048\omega_0$, in agreement with the anticipated value of $2\sqrt{1/\pi\alpha} \approx 0.047\omega_0$ suggested by our theoretical analysis. Hence, the frequency-domain photonic-channel analysis correctly describes the experimental findings.

Further Increase of the HHG peaks bandwidth requires the pulses entering the interferometer to have a larger bandwidth, which was obtained by generating short, 11fs pulses in a HCF, and subsequent compression on chirped mirrors (PC70 by *Ultrafast Innovations*). The two driver pulses exiting the interferometer had central

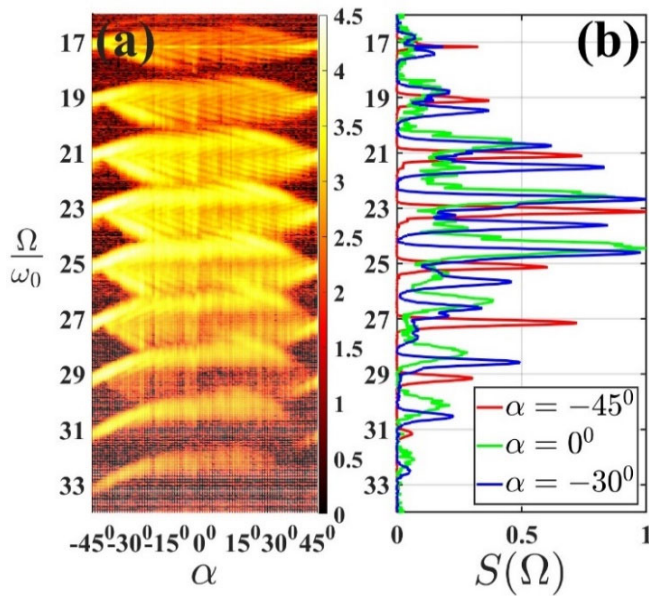


Fig. 4. (a) HGS intensity (logarithmic scale, maximal reading corresponds to 60000counts/sec) vs. harmonic order and angle α ; The spectrum of the two-color driver which exit the interferometer is given by the orange and red curves of Fig. 1(b). (b) HGS lineouts from (a) at $\alpha = -45^\circ$ (red curve), $\alpha = 0^\circ$ (green curve), $\alpha = -30^\circ$ (perpendicularly-elliptically polarized drivers, blue curve).

wavelengths of $\lambda_1 = 752\text{nm}$ and $\lambda_2 = 825\text{nm}$ (see Fig. 1b), same energy ($150\mu\text{J}$) and pulse durations of 16fs and 28fs respectively. As is evident from Fig. 4, increasing the difference between the central frequencies of the 2 arms $\omega_1 - \omega_2$, extends the span of harmonic channels such that channels emerging from adjacent odd-integer values get nested one into another to the extent that for any practical purposes a supercontinuum is obtained for $-25^\circ < \alpha < 25^\circ$. For comparison, driving HHG directly with the short linearly-polarized 11fs driver pulses yields bandwidth of only half an harmonic order (0.6eV) for each odd harmonic peak.

Finally, we exclude alternative explanations for the observed peak broadening. The moderate laser intensities used, together with absence of any noticeable HGS blueshift, redshift or peak broadening [25-28] of the channels (even for the cases $\alpha = \pm 45^\circ$) suggest that the intensity-dependent atomic phase is not the cause for the broadening, and that spatio-spectral effects are negligible [29]. Moreover, a synthesized Fourier-transform-limited vectorial driver (corresponding to the spectra in Fig. 1a assuming flat spectral phase) yields roughly the same peak intensity [for those instants relevant for recollision (where the field polarization is close to linear)] for all values of α . This excludes maker fringes [30] as a possible cause for the peak broadening. The focusing geometry favors the generation of the short quantum trajectories, which rules out broadening due to contribution of the long trajectories [31] or quantum path interferences [32]. Hence, the observed broadening reflects a genuine generation mechanism of new photonic channels.

Funding. Israel Science Foundation (524/19).

Acknowledgments. We thank Prof. Oren Cohen and Dr. Pavel Sidorenko for assistance with the FROG Ptychographic retrieval algorithm (<https://oren.net.technion.ac.il/ptych-frog/>).

Disclosures. The authors declare no conflicts of interest.

Data availability. Data underlying the results presented in this paper may be obtained from the authors upon reasonable request.

References

1. P. Corkum and F. Krausz, Nat. Phys. **3** 381 (2007).
2. F. Krausz and M. Ivanov, Rev. Mod. Phys. **81** 545 (2009).
3. J. Li, J. Lu, A. Chew, S. Han, J. Li, Y. Wu, H. Wang, S. Ghimire and Z. Chang, Nat. Comm. **11** 2748 (2020).
4. O. Kfir, S. Zayko, C. Nolte, M. Sivis, M. Möller, B. Hebler, S. S. P. K. Arekapudi, D. Steil, S. Schäfer, M. Albrecht, O. Cohen, S. Mathias and Claus Ropers, Science advances **3**.12 (2017): eaao4641.
5. J. Miao, T. Ishikawa, I. K. Robinson, M. M. Murnane, Science **348**, 530 (2015).
6. E. R. Shanblatt, C. L. Porter, D. F. Gardner, G. F. Mancini, R. M. Karl, Jr., M. D. Tanksalvala, C. S. Bevis, V. H. Vartanian, H. C. Kapteyn, D. E. Adams, and M. M. Murnane, Nano Lett. **16** 5444 (2016).
7. R. Geneaux, H. J. B. Marroux, A. Guggenmos, D. M. Neumark and S. R. Leone, Philosophical Transactions of the Royal Society A **377** 20170463 (2019).
8. H. Wang, M. Chini, S. Chen, C.-H. Zhang, F. He, Y. Cheng, Y. Wu, U. Thumm, and Z. Chang, Phys. Rev. Lett. **105** 143002 (2010).
9. P. Peng, C. Marceau, M. Hervé, P.B. Corkum, A. Yu. Naumov and D. M. Villeneuve, Nat. Comm. **10** 5269 (2019).
10. E. Goulielmakis, M. Schultze, M. Hofstetter, V. S. Yakovlev, J. Gagnon, M. Uiberacker, A. L. Aquila, E. M. Gullikson, D. T. Attwood, R. Kienberger, F. Krausz and U. Kleineberg, Science **320** 1614 (2008).
11. P. B. Corkum, N. H. Burnett and M. Y. Ivanov, Opt. Lett. **19** 1870 (1994).
12. V. T. Platonenko and V. V. Strelkov, J. Opt. Soc. Am. B **16** 435 (1999).
13. O. Tcherbakoff, E. Mével, D. Descamps, J. Plumridge and E. Constant, Phys. Rev. A **68** 043804 (2003).
14. B. Shan, S. Ghimire and Z. Chang, J. Mos. Opt. **52** 277 (2005).
15. Z. Chang, Phys. Rev. A **76** 051403(R) (2007).
16. X. Feng, S. Gilbertson, H. Mashiko, H. Wang, S. D. Khan, M. Chini, Y. Wu, K. Zhao, and Z. Chang, Phys. Rev. Lett. **103** 183901 (2009).
17. A. Fleischer and N. Moiseyev, Phys. Rev. A **74** 053806 (2006).
18. H. Merdji, T. Auguste, W. Boutu, J.-P. Caumes, B. Carré, T. Pfeifer, A. Jullien, D. M. Neumark and S. R. Leone, Opt. Lett. **32** 3134 (2007).
19. E. A. Khazanov, Quant. Elec. **52** 208 (2022).
20. M. Nisoli, S. DeSilvestri and O. Svelto, Appl. Phys. Lett. **68**, 2793 (1996).
21. M. Dorner-Kirchner, V. Shumakova, G. Coccia, E. Kaksis, B. E. Schmidt, V. Pervak, A. Pugzlys, A. Baltuška, M. Kitzler-Zeiler and P. A. Carpeggiani, ACS Photonics **10** 84 (2023).
22. A. Fleischer, O. Kfir, T. Diskin, P. Sidorenko and O. Cohen, Nat. Photon. **8** 543 (2014).
23. A. Fleischer, E. Bordo, O. Kfir, P. Sidorenko and O. Cohen, J. Phys. B **50** 034001 (2017).
24. E. Ragonis, E. Ben-Arosh, L. Merensky and A. Fleischer, in preparation.
25. J. B. Watson, A. Sanpera and K. Burnett, Phys. Rev. A **51** 1458 (1995).
26. H. J. Shin, D. G. Lee, Y. H. Cha, K. H. Hong and C. H. Nam, Phys. Rev. Lett. **83** 2544 (1999).
27. E. Brunetti, R. Issac, and D. A. Jaroszynski, Phys. Rev. A **77** 023422 (2008).
28. X.-B. Bian and A. D. Bandrauk, Appl. Sci. **3** 267 (2013).
29. A. Dubrouil, O. Hort, F. Catoire, D. Descamps, S. Petit, E. Mével, V.V. Strelkov and E. Constant, Nat. Comm. **5** 4637 (2014).
30. C. M. Heyl, J. Güdde, U. Höfer, and A. L'Huillier, Phys. Rev. Lett. **107** 033903 (2011).
31. X. He, M. Miranda, J. Schwenke, O. Guilbaud, T. Ruchon, C. Heyl, E. Georgadiou, R. Rakowski, A. Persson, M. B. Gaarde, and A. L'Huillier, Phys. Rev. A **79** 063829 (2009).
32. A. Zair, M. Holler, A. Guandalini, F. Schapper, J. Biegert, L. Gallmann, U. Keller, A. Wyatt, A. Monmayrant, I. A. Walmsley, E. Cormier, T. Auguste, J. P. Caumes and P. Salières, Phys. Rev. Lett. **100** 143902 (2008).

References (including paper titles)

1. P. Corkum and F. Krausz, "Attosecond Science", *Nat. Phys.* **3** 381 (2007).
2. F. Krausz and M. Ivanov, "Attosecond Physics", *Rev. Mod. Phys.* **81** 545 (2009).
3. J. Li, J. Lu, A. Chew, S. Han, J. Li, Y. Wu, H. Wang, S. Ghimire and Z. Chang, "Attosecond science based on high harmonic generation from gases and solids", *Nat. Comm.* **11** 2748 (2020).
4. O. Kfir, S. Zayko, C. Nolte, M. Sivils, M. Möller, B. Hebler, S. S. P. K. Arekapudi, D. Steil, S. Schäfer, M. Albrecht, O. Cohen, S. Mathias and Claus Ropers, "Nanoscale magnetic imaging using circularly polarized high-harmonic radiation", *Science advances* **3**.12 (2017): eaao4641.
5. J. Miao, T. Ishikawa, I. K. Robinson, M. M. Murnane, "Beyond crystallography: Diffractive imaging using coherent X-ray light sources", *Science* **348**, 530 (2015).
6. E. R. Shanblatt, C. L. Porter, D. F. Gardner, G. F. Mancini, R. M. Karl, Jr., M. D. Tanksalvala, C. S. Bevis, V. H. Vartanian, H. C. Kapteyn, D. E. Adams, and M. M. Murnane, "Quantitative Chemically Specific Coherent Diffractive Imaging of Reactions at Buried Interfaces with Few Nanometer Precision", *Nano Lett.* **16** 5444 (2016).
7. R. Geneaux, H. J. B. Marroux, A. Guggenmos, D. M. Neumark and S. R. Leone, "Transient absorption spectroscopy using high harmonic generation: a review of ultrafast X-ray dynamics in molecules and solids", *Philosophical Transactions of the Royal Society A* **377** 20170463 (2019).
8. H. Wang, M. Chini, S. Chen, C.-H. Zhang, F. He, Y. Cheng, Y. Wu, U. Thumm, and Z. Chang, "Attosecond Time-Resolved Autoionization of Argon", *Phys. Rev. Lett.* **105** 143002 (2010).
9. P. Peng, C. Marceau, M. Hervé, P.B. Corkum, A. Yu. Naumov and D. M. Villeneuve, "Symmetry of molecular Rydberg states revealed by XUV transient absorption spectroscopy", *Nat. Comm.* **10** 5269 (2019).
10. E. Goulielmakis, M. Schultze, M. Hofstetter, V. S. Yakovlev, J. Gagnon, M. Uiberacker, A. L. Aquila, E. M. Gullikson, D. T. Attwood, R. Kienberger, F. Krausz and U. Kleineberg, "Single Cycle Nonlinear Optics", *Science* **320** 1614 (2008).
11. P. B. Corkum, N. H. Burnett and M. Y. Ivanov, "Subfemtosecond pulses", *Opt. Lett.* **19** 1870 (1994);
12. V. T. Platonenko and V. V. Strelkov, "Single attosecond soft-x-ray pulse generated with a limited laser beam", *J. Opt. Soc. Am. B* **16** 435 (1999).
13. O. Tcherbakoff, E. Mével, D. Descamps, J. Plumridge and E. Constant, "Time-gated high-order harmonic generation", *Phys. Rev. A* **68** 043804 (2003).
14. B. Shan, S. Ghimire and Z. Chang, "Generation of the attosecond extreme ultraviolet supercontinuum by a polarization gating", *J. Mos. Opt.* **52** 277 (2005).
15. Z. Chang, "Controlling attosecond pulse generation with a double optical gating", *Phys. Rev. A* **76** 051403 (R) (2007).
16. X. Feng, S. Gilbertson, H. Mashiko, H. Wang, S. D. Khan, M. Chini, Y. Wu, K. Zhao, and Z. Chang, "Generation of Isolated Attosecond Pulses with 20 to 28 Femtosecond Lasers", *Phys. Rev. Lett.* **103** 183901 (2009).
17. A. Fleischer and N. Moiseyev, "Attosecond laser pulse synthesis using bichromatic high-order harmonic generation", *Phys. Rev. A* **74** 053806 (2006).
18. H. Merdji, T. Augustine, W. Boutu, J.-P. Caumes, B. Carré, T. Pfeifer, A. Jullien, D. M. Neumark and S. R. Leone, "Isolated attosecond pulses using a detuned second-harmonic field", *Opt. Lett.* **32** 3134 (2007).
19. E. A. Khazanov, "Post-compression of femtosecond laser pulses using self-phase modulation: from kilowatts to petawatts in 40 years", *Quant. Elec.* **52** 208 (2022).
20. M. Nisoli, S. DeSilvestri and O. Svelto, "Generation of high energy 10 fs pulses by a new pulse compression technique", *Appl. Phys. Lett.* **68**, 2793 (1996).
21. M. Dorner-Kirchner, V. Shumakova, G. Coccia, E. Kaksis, B. E. Schmidt, V. Pervak, A. Pugzlys, A. Baltuška, M. Kitzler-Zeiler and P. A. Carpeggiani, "HHG at the Carbon K-Edge Directly Driven by SRS Red-Shifted Pulses from an Ytterbium Amplifier", *ACS Photonics* **10** 84 (2023).
22. A. Fleischer, O. Kfir, T. Diskin, P. Sidorenko and O. Cohen, "Spin angular momentum and tunable polarization in high harmonic generation", *Nat. Photon.* **8** 543 (2014).
23. A. Fleischer, E. Bordo, O. Kfir, P. Sidorenko and O. Cohen, "Polarization-fan high-order harmonics", *J. Phys. B* **50** 034001 (2017).
24. E. Ragonis, E. Ben-Arosh, L. Merensky and A. Fleischer, in preparation.
25. J. B. Watson, A. Sanpera and K. Burnett, "Pulse-shape effects and blueshifting in the single-atom harmonic generation from neutral species and ions", *Phys. Rev. A* **51** 1458 (1995).
26. H. J. Shin, D. G. Lee, Y. H. Cha, K. H. Hong and C. H. Nam, "Generation of Nonadiabatic Blueshift of High Harmonics in an Intense Femtosecond Laser Field", *Phys. Rev. Lett.* **83** 2544 (1999).
27. E. Brunetti, R. Issac, and D. A. Jaroszynski, "Quantum path contribution to high-order harmonic spectra", *Phys. Rev. A* **77** 023422 (2008).
28. X.-B. Bian and A. D. Bandrauk, "Spectral Shifts of Nonadiabatic High-Order Harmonic Generation", *Appl. Sci.* **3** 267 (2013).
29. A. Dubrouil, O. Hort, F. Catoire, D. Descamps, S. Petit, E. Mével, V.V. Strelkov and E. Constant, "Spatio-spectral structures in high-order harmonic beams generated with Terawatt 10-fs pulses", *Nat. Comm.* **5** 4637 (2014).
30. C. M. Heyl, J. Güdde, U. Höfer, and A. L'Huillier, "Spectrally Resolved Maker Fringes in High-Order Harmonic Generation", *Phys. Rev. Lett.* **107** 033903 (2011).
31. X. He, M. Miranda, J. Schwenke, O. Guilbaud, T. Ruchon, C. Heyl, E. Georgadiou, R. Rakowski, A. Persson, M. B. Gaarde, and A. L'Huillier, "Spatial and spectral properties of the high-order harmonic emission in argon for seeding applications", *Phys. Rev. A* **79** 063829 (2009).
32. A. Zair, M. Holler, A. Guandalini, F. Schapper, J. Biegert, L. Gallmann, U. Keller, A. Wyatt, A. Monmayrant, I. A. Walmsley, E. Cormier, T. Augustine, J. P. Caumes and P. Salières, "Quantum Path Interferences in High-Order Harmonic Generation", *Phys. Rev. Lett.* **100** 143902 (2008).